AIP Advances

Method for determining the thermal conductivity of *in situ* formation rock using drilling cuttings

Cite as: AIP Advances **11**, 065015 (2021); https://doi.org/10.1063/5.0051586
Submitted: 26 March 2021 • Accepted: 24 May 2021 • Published Online: 10 June 2021

Fu Yi, Xupeng Qi, Xuexin Zheng, et al.

Method for determining the thermal conductivity of *in situ* formation rock using drilling cuttings

Cite as: AIP Advances 11, 065015 (2021); doi: 10.1063/5.0051586
Submitted: 26 March 2021 • Accepted: 24 May 2021 •
Published Online: 10 June 2021

Fu Yi,[1] Xupeng Qi,[2,a)] Xuexin Zheng,[3] Huize Yu,[3] Wenming Bai,[4] and Hanbo Bao[4]

AFFILIATIONS

[1] College of Architecture and Transportation, Liaoning Technical University, Fuxin 123000, China
[2] School of Civil Engineering, Liaoning Technical University, Fuxin 123000, China
[3] Changchun High New Technology Building Development, Inc., Changchun 130000, China
[4] Lutekunzhe Energy Technology Co., Ltd., Changchun 130000, China

[a)] **Author to whom correspondence should be addressed:** qixupeng007@163.com

ABSTRACT

In this paper, a method for determining the thermal conductivity of *in situ* formation rock, which combines experimental measurements, theoretical model predictions, and geophysical logging of formation porosity, is presented to predict the thermal conductivity of *in situ* formation rocks (this method effectively combines experimental measurements, theoretical model, and geological conditions, referred to as "ETG," where E is for experimental measurements, T is for the theoretical model, and G is for geological conditions). 24 drilling cuttings samples from rocks down to a depth of 2000 m were selected for transient plane source thermal conductivity tests, and an effective thermal conductivity method was used to predict the thermal conductivity of rocks corresponding to each formation. The predicted thermal conductivity of mudstone was 2.31–3.27 W/(m K), and that of sandstone was 2.40–3.69 W/(m K). An independent-samples t test was carried out between the thermal conductivity results from the ETG prediction method and those from a diagenetic mineral-theory model. The results showed that there were no statistically significant differences between the two groups ($P > 0.05$) and that the fitting degree was high. The mean-square error in the solid thermal conductivities determined by the two methods was about 0.3, which indirectly demonstrates that the ETG method has high accuracy for predicting the thermal conductivity of *in situ* formation rock. Therefore, this method is likely to become popular in engineering practice.

I. INTRODUCTION

Disastrous events brought about by global warming are increasing year by year. The process of replacing traditional fossil-fuel energy with clean and renewable energy is accelerating continuously. Using geothermal energy to cool and heat buildings has become an area of significant research in recent years.[1,2] Medium-depth geothermal heat-pump technology has the characteristics of stable heat-transfer performance and large heat extraction from a single hole, and it is gradually becoming an important source of winter heating and a heat source in cold-climate areas.[3] The thermal conductivity of rock is an important factor for evaluating the suitability of an area for the application of ground-source heat pumps (GSHPs), and this is also a decisive factor for determining the heat-transfer effect of GSHPs.[4]

Many experts and scholars have made outstanding contributions to the key problem of determining the thermal conductivity of rocks. In 1886, French mathematician and physicist Joseph Fourier summarized his experimental results by producing a principle and method for determining the thermal conductivity coefficient of a material, defining the heat-transfer equation. On this theoretical basis, later generations have continuously innovated, inventing a variety of methods for measuring the thermal conductivity of rocks, and these can be broadly divided into steady-state and transient methods.[5] Steady-state test methods require the heat flow from a heating plate to pass vertically through the cross section of a core sample under test. Although this method has high accuracy, it is unpopular in engineering applications due to the difficulty of core extraction, the requirement for high-quality sample processing, and its long testing time. In contrast, transient test methods assume that the probe–sample contact is a one-dimensional steady-state heat-transfer problem, and the thermal conductivity of the rock than then be inferred by measuring the thermal diffusivity of the rock. This type of method is the first choice for the measurement of drilling cuttings because it has a short measurement time and can also be used to measure the thermal conductivity of powdered samples.

Using the principle of unsteady heat transfer, Kämmlein and Stollhofen[6] employed a probe method to calculate the thermal conductivities of materials by measuring the temperature change with time when a linear heat source is acting on a quasi-infinite uniform medium. They applied this technique to measuring the thermal conductivity of drilling cuttings and found that the particle size distribution was the main factor affecting the porosity of the rock, while the particle size had little influence on the thermal conductivity, and the mineral composition was the main factor affecting the thermal conductivity of rock powder. Although this probe method is convenient and rapid, the small contact area between the probe and the cuttings leads to relatively large measurement errors.

The principle of the transient plane heat source (TPS) method to measure the thermal conductivity of cuttings is based on the transient temperature response generated by a disk-shaped heat source with step heating in an infinite medium. The method has good accuracy and repeatability, but it measures the thermal conductivity of rock cuttings, and this does not directly represent the thermal conductivity of undisturbed rock.[7,8] Rocks and their powders are typical porous media composed of a solid phase with fluid in the pores. The thermal conductivity of the solid phase is much larger than that of the fluid in the pores, so changing the porosity of the rock has a great influence on its thermal conductivity.[9] In the process of sampling and transportation, secondary damage to cores cannot be avoided, and this will lead to changes in the internal pores of a core, in turn leading to reduced accuracy of the thermal conductivity measurements in the laboratory. To avoid the impact of secondary cracks caused by field coring on the accuracy of the measurement of the thermal conductivity of rock *in situ*, some scholars have tried to establish a relationship between longitudinal waves and the thermal conductivity of rock so that its thermal conductivity can be predicted.[10,11] This kind of method is based on a large amount of data, and it is therefore difficult to collect data in its early stages. In addition, the principle of the method has no physical significance and is only a mathematical relationship between sample data.

Some scholars regarded rocks as porous media, so diagenetic minerals were a solid phase, and water in pores was divided into a liquid phase. A mathematical model to predict the thermal conductivity of rock by calculating the resistance in a circuit according to the different thermal conductivities of a two-phase medium has been put forward.[12] Golden and Papanicolaou proposed a boundary series–parallel model, which assumes that the direction of heat flow and the direction of the heat-resistance arrangement can be regarded as a series and parallel arrangement of resistors in a circuit, under the premise that the volume content of the rock components and the thermal conductivity of each component are known. The principle of this method is simple, but it is only suitable for predicting a range of thermal conductivity.[13] Eucken applied Maxwell's resistivity-prediction model to the prediction of the thermal conductivity of rock. This method can only be used when the thermal conductivities of the discrete phases are similar.[14] Fiala *et al.* established a calculation model for the thermal conductivity of cement-based materials assuming a solid skeleton based on the effective-medium (approximate) theory.[15] Johansen proposed a generalized geometric-mean method to predict thermal conductivity.[16] This model involves a mathematical processing method, but it lacks actual physical significance; however, because its predicted values are highly consistent with the measured values, it is currently the most widely used prediction model.

Some scholars have also proposed new assumptions on the basis of satisfying the above single model and have thus put forward a combined model. Hashin and Shtrikman introduced a weight coefficient, substituted the structural proportionality coefficient for the component proportionality coefficient, and proposed a weighted harmonic-average model based on the series–parallel model.[17,18] Laurent introduced a coefficient related to the skeleton structure to represent the proportion of the structure forming parallel thermal resistance, and they proposed a composite structure model for the thermal conductivity of porous media.[19] Although their combined model has high accuracy, it is not popular in engineering practice because of its complexity and the difficulty in parameter determination in the model.

In the past, scholars have focused their research on the accuracy of thermal conductivity measurements of samples, but there have been few studies on the prediction of the thermal conductivity of *in situ* formation rocks from drilling cuttings. However, sampling of drilling cuttings is relatively convenient for practical engineering, and core-drilling is comparatively difficult and the cost of obtaining cores from medium-depth and deep formations is high. Therefore, it is of great significance to develop a method for predicting the thermal conductivity of *in situ* formation rock using the thermal conductivity of drilling cuttings. In this paper, a method (ETG) is proposed to predict the thermal conductivity of rock *in situ*. This is based on a combination of laboratory tests, theoretical model prediction, geophysical logging of the formation porosity, and studying thermal conductivity tests and prediction models for drilling cuttings.

II. EXPERIMENTAL AND MODELING METHODS

Drilling cuttings are small particles formed by cutting rocks with a drill bit in the process of drilling. Their diameter is generally less than 2 mm. A drilling core is a cylindrical rock sample obtained from underground using a coring bit in drilling engineering. Compared with drilling core sampling, drilling cuttings are more convenient and cheaper to collect, making them ideal for predicting the thermal conductivity of rocks. However, the particle sizes and shapes present in these cuttings are affected by many factors, such as the rock's hardness and mineral composition, the drilling rate, and the drill bit pressure, and this needs to be considered. Relevant studies have shown that the particle size distribution is the main factor affecting the thermal conductivity of such rock debris. However, when the particle size is less than 0.075 mm, the particle size distribution has a negligible influence on the thermal conductivity.[6] In this study, the thermal conductivity of saturated rock powder was examined experimentally, and the thermal conductivity of *in situ* formation rock was calculated according to the experimental results combined with a prediction model considering the formation porosity.

A. ETC thermal conductivity calculation process

A flowchart of the calculation process to determine the required parameters of the *in situ* rock thermal conductivity prediction model is shown in Fig. 1.

B. Measurement of thermal conductivity of saturated cuttings

1. Sample preparation

The samples were selected from drilling cuttings obtained during the construction of a deep-buried pipe heat-exchange well (depth 2000 m) in Changchun Modern Logistics Building Project, China. The cuttings were dried and then ground to powder with particles with diameters less than 0.075 mm (hereafter referred to as cuttings powder) using a grinding machine [as shown in Fig. 3(a)]. A total of 200 g of the dry drilling cuttings was sealed for use. In this study, a scanning electron microscope (SEM; FEI Quanta 450) was used to observe the detailed profiles of 24 samples from the Songliao Basin (located in the northeast of China). It was found that when the particle diameter was <0.075 mm, the shapes of the powder particles were similar and consistent (approximately circular or oval), and the influence of the particle profile on the experimental results could therefore be ignored, as shown in Fig. 2.

2. Experimental principle

These experiments were completed in the laboratory of Jilin Jianzhu University using a Hot Disk TPS 2500 S thermal constant analyzer [as shown in Fig. 3(c)]. This device can measure the thermal properties of materials, and it is based on the TPS principle described earlier. The experimental setup (Fig. 3) mainly included the Hot Disk data-acquisition instrument, and a heating probe, fixing frame, beaker, and computer. The probe is composed of a nickel helix sensor with conductive double-helix structure winding wire, and this encapsulated nickel helix sensor is clamped into the sample (powder or liquid). The sensor acts both as a heat source to increase the temperature and as a heat-flux resistance meter to record the temperature rise with time. When a constant power P is output, a temperature field is generated through the direct current of the sensor, and this generates a stepped heat pulse inside the sample. The thermal conductivity of the rock is then calculated by the temperature curves of the probe and the sample.[7] The relationship between the increase of the temperature to which the sample is heated and the effective heating time can be expressed by

$$R(t) = R_0\left[1 + \alpha\Delta T'\left(\sqrt{\frac{t\kappa}{r^2}}\right)\right], \tag{1}$$

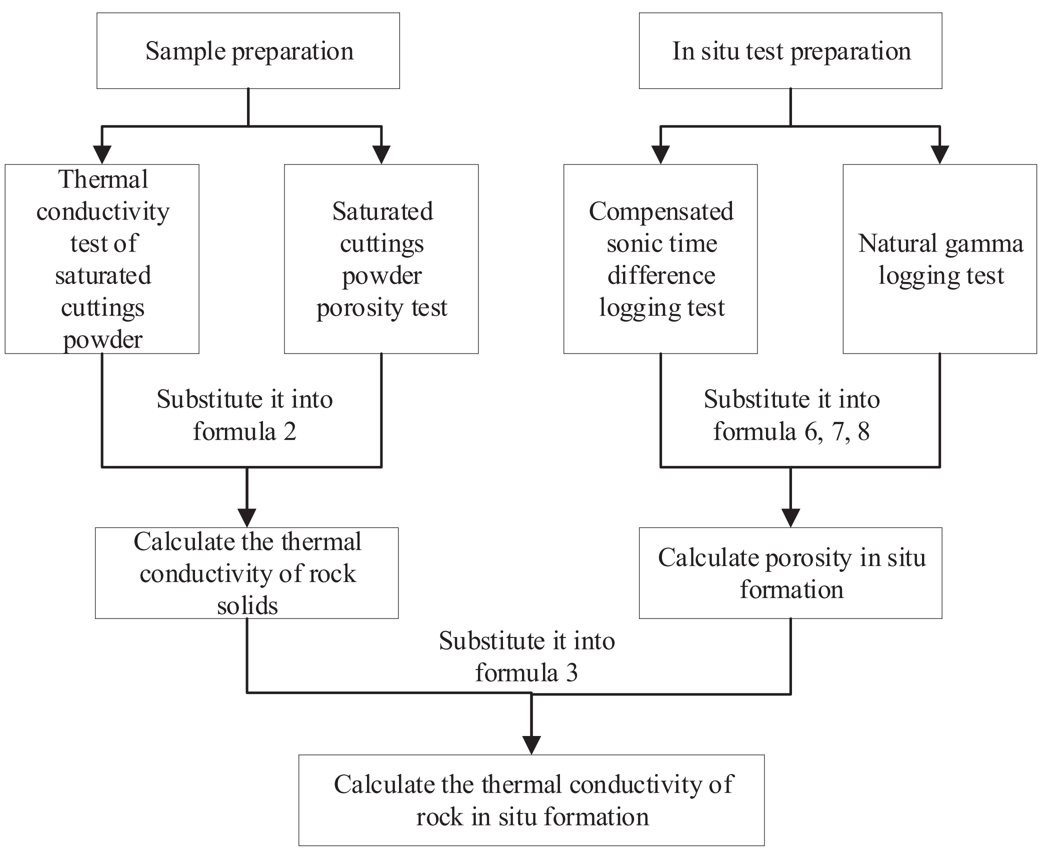

FIG. 1. Process for calculating the ETC thermal conductivity.

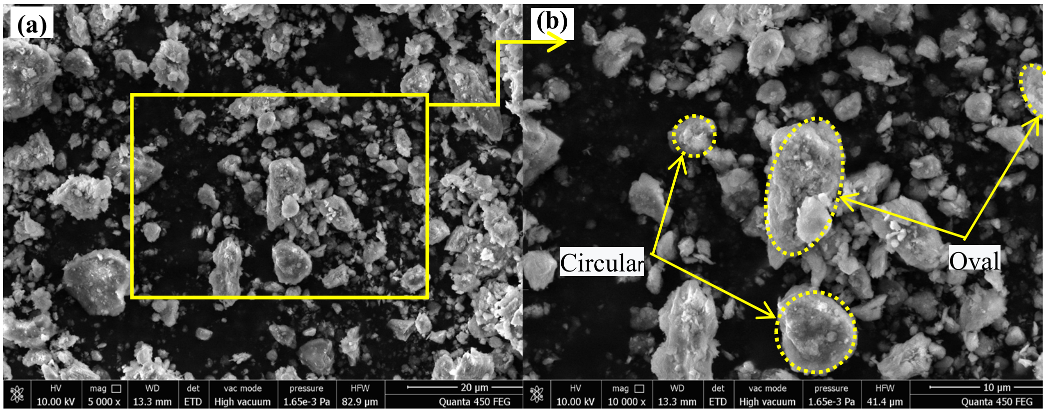

FIG. 2. SEM images of cuttings powder at magnifications of (a) 5000 times and (b) 10 000 times.

where $R(t)$ is the change in the resistance with the time after the nickel helix sensor is heated; R_0 is the initial resistance of the nickel helix sensor before heating; α is the resistance temperature coefficient; t is the heating time; κ is the sample thermal diffusivity; r is the radius of sensor; and $\Delta T'$ is the temperature rise on the other side of the insulation layer and the side facing the nickel helical sensor of the rock sample surface.

The thermal conductivity measurement range of the experimental instrument is 0.01–500 W/(m K), and its accuracy is greater than 0.1 W/(m K), and the measured temperature should not exceed 1000 K. The measurement data processing software used was Hot Disk TPS 2500S Thermal Constant Analyzer v6.0.

3. Measuring the thermal conductivity of cuttings powder

To measure the thermal conductivity, 200 g of finely ground rock powder was put into a beaker, and water was added while stirring until it reached saturation. Absorbent paper was used to absorb

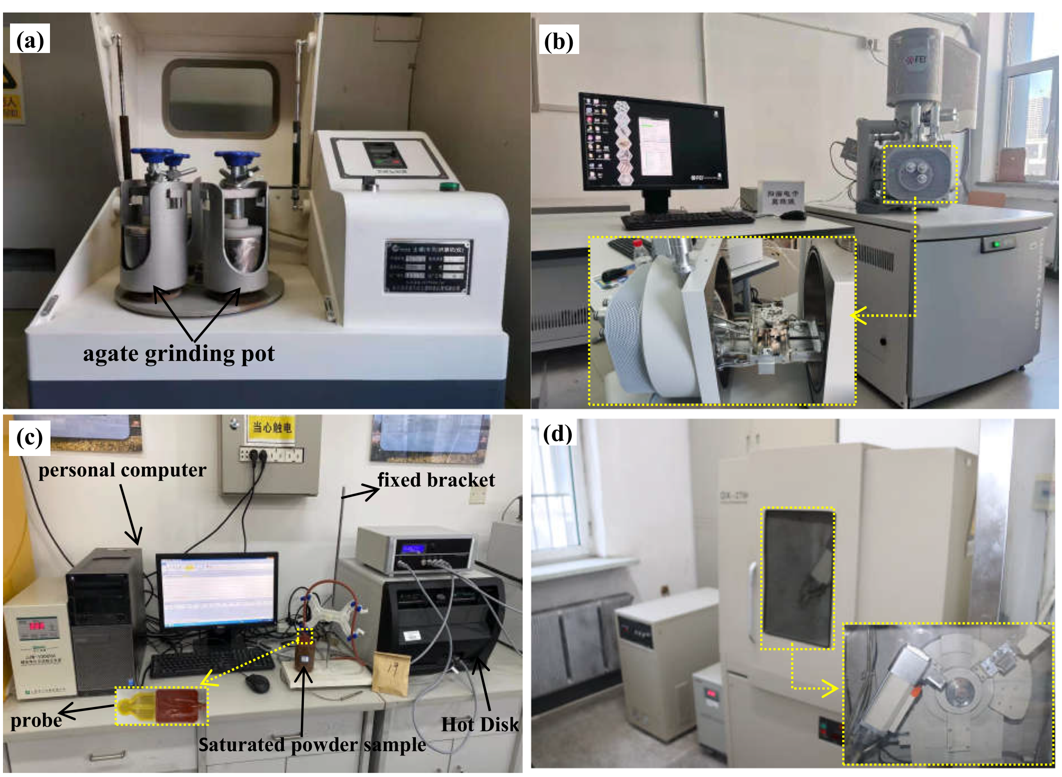

FIG. 3. Experimental equipment: (a) grinding instrument, (b) scanning electron microscope, (c) Hot Disk thermal constant tester, and (d) x-ray diffraction instrument.

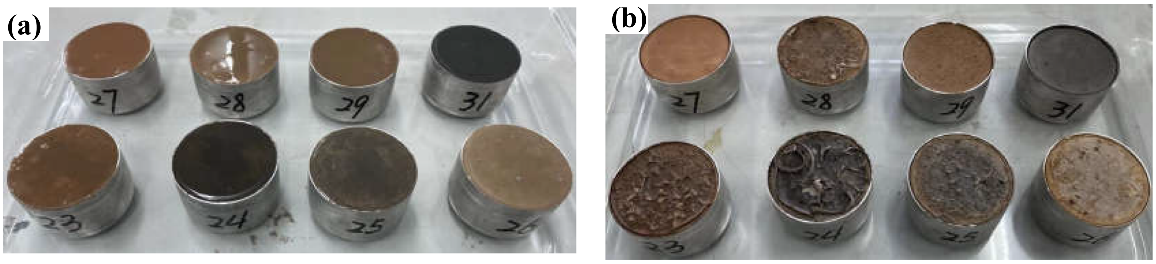

FIG. 4. Powder samples (a) before and (b) after drying.

excess water from the surface of the sample. At this point, the sample powder in the beaker was considered to be saturated, and the pore areas of the *in situ* rock are usually water saturated.[6] The Hot Disk probe was then inserted vertically into the beaker powder sample, the probe sensing line was fixed onto the mounting frame, and the probe's double helix center was kept in line with the geometric center of the powder in the beaker [as shown in Fig. 3(c)]. This was then left to stand for 1 h. The test parameters were set (the test voltage was 0.03 W, and the test duration was 160 s), the measurement was started, and the results were recorded when it had finished.

C. Determination of the porosity of the saturated cuttings

The porosity of the cuttings refers to the percentage of their pores that are filled with water as a fraction of the total volume of the saturated powder. After the thermal conductivity tests of the saturated cuttings were completed, the saturated cuttings in the geometric center area of the sample in the beaker were taken out and poured into an aluminum pan until it was full, as shown in Fig. 4. The total weight of the aluminum pan and the saturated powder sample was measured as m_1. The aluminum pans filled with sample rock were placed into an oven to dry, and the total mass of the powder sample and the aluminum pan after drying was recorded as m_2. Assuming that the influence of moisture in the air on the mass of the dried cuttings can be ignored, the mass difference before drying can be considered as the mass of the pore water in the cuttings powder. Given the density of water at the laboratory temperature, Eq. (2) was used to calculate the porosity of the saturated rock powder samples,

$$\varphi_s = \frac{(m_1 - m_2)}{\rho_w V}, \tag{2}$$

where ϕ_s is the percentage porosity of the saturated cuttings at the laboratory temperature, %; ρ_w is the density of water at the laboratory temperature in g/cm^3; and V is the volume of the aluminum pot in L. In this case, the volume of the aluminum pots selected was 0.06 L.

D. Determination of the porosity of *in situ* formation rock

The porosity of *in situ* formation rock refers to the ratio of fluid to its total volume. *In situ* rock porosity measurements were performed using the SDZ-3000 fast logging platform. The SDZ-3000 consists of a surface logging system and a downhole instrument, as shown in Fig. 5.

The surface logging system can monitor a series of downhole instruments (compensated acoustic wave and natural gamma ray sensors in this case) in real time, and it uses dual Manchester code communication technology, which allows two-way data communication between the surface system and the downhole instruments.[20] The acoustic probe, which consists of one transmitter and four receivers, releases an acoustic wave through the transmitter, and the

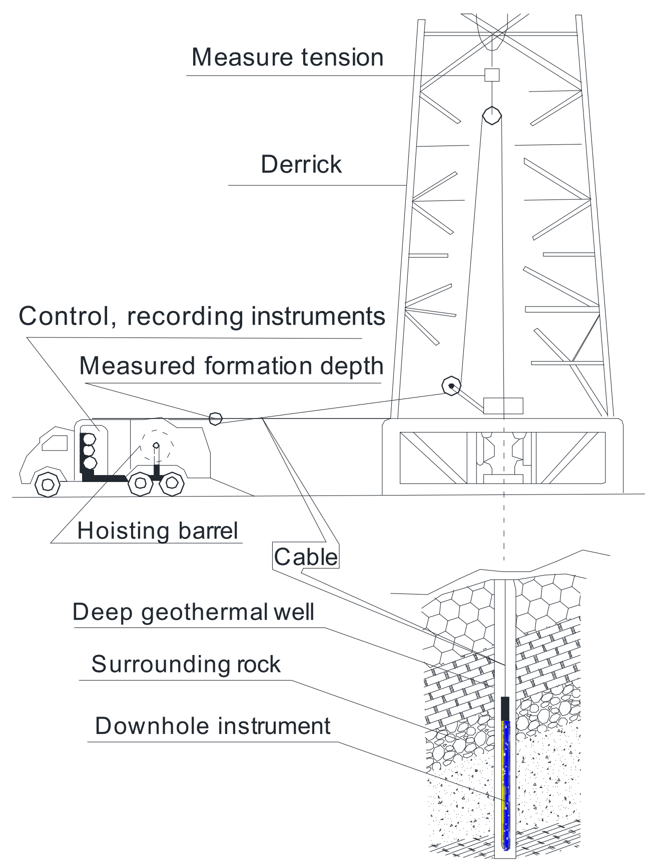

FIG. 5. Diagram of the SDZ-3000 logging system.

receivers receive the acoustic wave, forming an electrical signal and transmitting it to the ground logging system through the cable to calculate the average value of the acoustic time difference obtained by the four receivers, and this is known as the acoustic compensated (AC) time difference curve. The total porosity of the formation is obtained by substituting the AC curve value into Eq. (4).

For gamma ray (GR) logging,[21] the detection instrument is put into the well by the logging truck. During the lifting process, the detector receives the gamma rays generated by the decay of radioactive elements and converts them into electrical pulse signals. After amplification, the gamma ray (GR) signals are transmitted to the surface logging system via the cable. The natural gamma value in the GR curve is substituted into Eq. (3) to calculate the impact factor of the mud content. The argillaceous content in the rock pores will reduce its porosity, so it is necessary to calculate the effective porosity of the rock to represent the actual porosity of the formation. The calculation for this is given in Eq. (5),

$$\lambda_{SH} = \frac{T_{GR} - T_{GR_{\min}}}{T_{GR_{\max}} - T_{GR_{\min}}}, \tag{3}$$

$$\varphi_{POR} = \frac{(T_{AC} - T_m)}{(T_f - T_m)} \times \frac{1}{\lambda_{CP}} \times \%, \tag{4}$$

$$\varphi_{PORR} = \varphi_{POR} - \lambda_{SH} \times \frac{T_{sh} - T_m}{T_f - T_m} \times \%. \tag{5}$$

In Eqs. (3)–(5), λ_{SH} is the mud content influencing factor; T_{GR} is the gamma ray log value, API (the unit of gamma ray log value); $T_{GR_{\min}}$ is the natural gamma value of pure sandstone, API; $T_{GR_{\max}}$ is the natural gamma value of pure mudstone, API; φ_{POR} is the total porosity of the formation, %; T_{AC} is the acoustic-compensated sonic time difference curve, μs/m; T_m is the sandstone frame time difference, μs/m; T_f is the fluid acoustic time difference, μs/m; λ_{CP} is the compaction correction factor; φ_{PORR} is the effective formation porosity, %; and T_{sh} is the mudstone acoustic time difference, μs/m.

E. ETG thermal conductivity prediction model

The saturated (or dry) rock can be considered as a two-phase porous medium consisting of a solid mineral phase with fluid in the pores between solid-phase particles, as shown in Fig. 6(a).[22] Under given measurement conditions, the thermal conductivity of the rock will be greatly different from that of the fluid, and the heat flow through the solid in the same area per unit time will be much greater than that through the fluid. The idea of series and parallel resistance calculations in a circuit was introduced to simplify a two-phase rock medium, and this simplified unit structure model is shown in Figs. 6(b) and 6(c). On this basis, previous researchers have derived many theoretical models to predict the thermal conductivity of rocks. By analyzing the two-phase theoretical models, the main factors that determine the prediction results of the model were obtained. These were the thermal conductivity of the solid phase, the thermal conductivity of the fluid, and the two-phase volume fraction.

Drilling cuttings are produced from the drill bit breaking the original rock into small pieces, and the mineral composition of the rock itself is not changed by this process. The cuttings can be approximately regarded as a porous granular material, and the thermal conductivity of the cuttings pile can be predicted using a theoretical model of heat and mass transfer in porous media. Therefore, the volume-averaging method can be used to establish the microscale characteristic unit structure, which comprises a solid matrix (skeleton or particles) and pores.

Under the condition that the thermal conductivity and the porosity of the rock cuttings are known, the thermal conductivity of the solid phase can be predicted by making use of the relationship between the porosity and the thermal conductivities of the solid and liquid phases. In this paper, a high-accuracy two-phase geometric-average model with wide applicability was selected as the theoretical prediction model. The calculation equations for this are

$$\lambda_h = {\lambda_s}^{(1-\varphi_s)} \cdot {\lambda_w}^{\varphi_s}, \tag{6}$$

$$\lambda_s = 10^{\frac{\log^{\lambda_h} - \log^{\lambda_s^{\varphi_s}}}{1-\varphi_s}}, \tag{7}$$

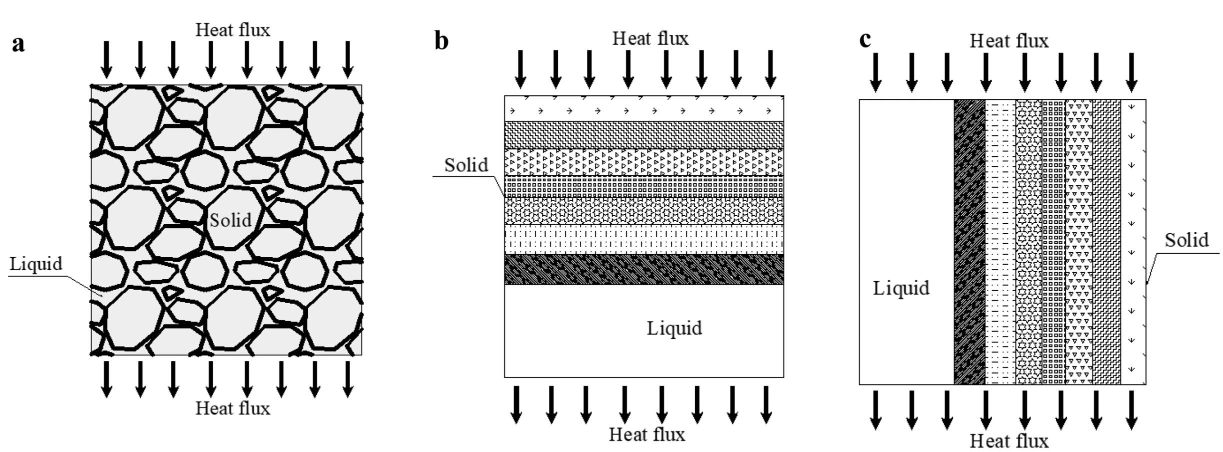

FIG. 6. Series and parallel distribution element structure models for saturated (or dry) rock with two media: (a) two-phase medium; (b) series model; (c) parallel model.

$$\lambda_{geo} = \lambda_s^{(1-\varphi_{PORR})} \cdot \lambda_w^{\varphi_{PORR}}, \tag{8}$$

where λ_h is the thermal conductivity of the saturated cuttings, W/(m K); λ_s is the thermal conductivity of the solid-phase rock, W/(m K); λ_w is the thermal conductivity of water under laboratory conditions, W/(m K); and λ_{geo} is the thermal conductivity of the *in situ* rock, W/(m K). By substituting the solid thermal conductivity of rock and the porosity of *in situ* formation rock into the theoretical model represented by Eq. (8), λ_{geo} can be calculated.

To sum up, the experimental parameters needed to determine the thermal conductivity of *in situ* formation rock include the thermal conductivity of the saturated cuttings powder, the porosity of the saturated cuttings powder, and the porosity of the *in situ* formation rock.

III. EXPERIMENTAL RESULTS

In this study, the ETG model was used to predict the *in situ* thermal conductivity of the rock in a middle-deep geothermal well (depth 2000 m) in a project in the north of Changchun, Songliao Basin. A total of 24 drilling cuttings samples were selected, and the corresponding formation depth range was 700–2000 m. Among these samples, 12 were mudstones (labeled No. M-1 to M-12) and 12 (labeled No. S-1 to S-12) were sandstones, as shown in Table I.

A. Laboratory test results

The thermal conductivity values of the saturated drilling cuttings powder samples, measured according to the method described in Sec. II B, are shown in Table I. The sample masses were measured according to the method in Sec. II C, and the calculated porosities of the saturated drilling cuttings samples are shown in Table II.

TABLE I. Measured thermal conductivities of saturated drilling cuttings samples.

No.	Depth (m)	λ_h [W/(m K)]	No.	Depth (m)	λ_h [W/(m K)]
M-1	730	1.14	S-7	1430	1.68
M-2	740	1.26	S-8	1450	1.79
M-3	770	1.21	S-9	1490	1.87
S-1	850	1.60	S-10	1500	1.79
S-2	930	1.88	S-11	1510	1.78
S-3	1090	1.86	S-12	1560	1.74
M-4	1150	1.41	M-7	1570	1.54
M-5	1170	1.66	M-8	1580	1.64
M-6	1340	1.23	M-9	1610	1.71
S-4	1360	1.59	M-10	1710	1.72
S-5	1380	1.88	M-11	1780	1.73
S-6	1400	1.88	M-12	1810	1.87

TABLE II. Calculated porosities of the saturated drilling cuttings samples.

No.	Saturated m_{1i} (g)	Dry m_{2i} (g)	φ_{si}	No.	Saturated m_{1i} (g)	Dry m_{2i} (g)	φ_{si}
M-1	109.80	82.35	0.46	S-1	122.43	101.84	0.34
M-2	112.09	86.86	0.42	S-2	120.97	100.00	0.35
M-3	113.09	86.07	0.45	S-3	124.29	103.07	0.35
M-4	114.97	89.91	0.42	S-4	120.47	98.79	0.36
M-5	121.17	99.26	0.37	S-5	125.20	107.19	0.30
M-6	114.04	87.77	0.44	S-6	128.29	110.03	0.30
M-7	119.93	97.85	0.37	S-7	122.53	104.53	0.30
M-8	121.95	100.45	0.36	S-8	120.89	101.12	0.33
M-9	123.97	103.16	0.35	S-9	121.78	103.21	0.31
M-10	123.98	103.01	0.35	S-10	122.20	101.23	0.35
M-11	120.10	96.91	0.39	S-11	119.19	98.22	0.35
M-12	119.07	95.19	0.40	S-12	122.37	100.20	0.37

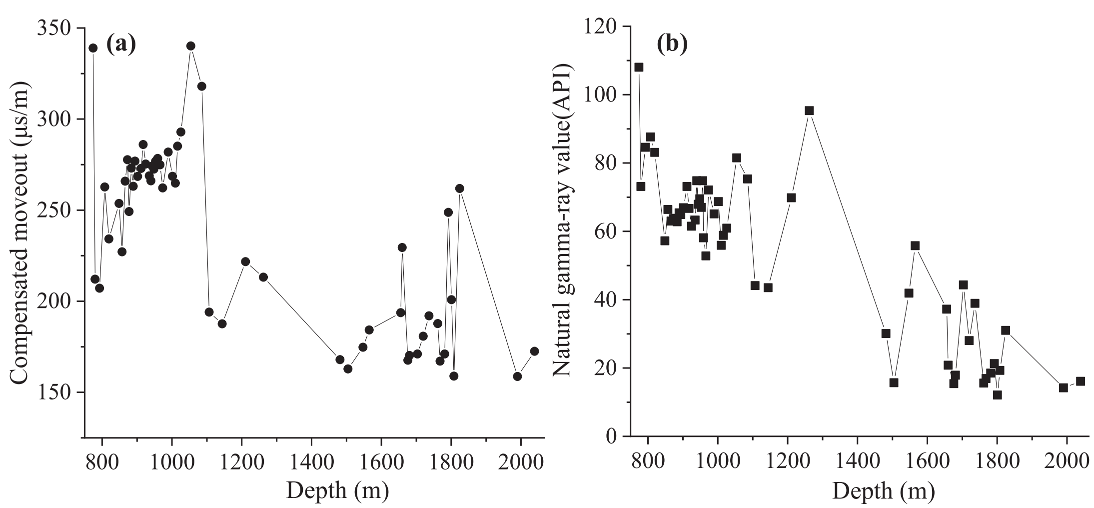

FIG. 7. Relationships between field logging values and well depth: (a) compensated acoustic time difference curve; (b) gamma ray log.

TABLE III. Effective porosities of *in situ* formations.

No.	φ_{PORR} (%)	No.	φ_{PORR} (%)
M-1	1.8	S-1	5.8
M-2	1.6	S-2	11.2
M-3	11.3	S-3	4.7
M-4	3.8	S-4	4.0
M-5	5.8	S-5	3.5
M-6	5.8	S-6	1.8
M-7	3.4	S-7	15.8
M-8	3.2	S-8	14.9
M-9	2.8	S-9	23.4
M-10	2.1	S-10	4.4
M-11	2.1	S-11	4.1
M-12	4.2	S-12	3.8

TABLE IV. Calculated thermal conductivities of *in situ* formation rocks.

No.	λ_{geo} [W/(m K)]	No.	λ_{geo} [W/(m K)]
M-1	2.56	S-1	2.76
M-2	2.62	S-2	2.73
M-3	2.31	S-3	2.40
M-4	2.9	S-4	2.89
M-5	2.67	S-5	3.23
M-6	2.78	S-6	3.69
M-7	3.05	S-7	2.18
M-8	3.13	S-8	2.77
M-9	3.22	S-9	2.37
M-10	3.27	S-10	3.01
M-11	3.20	S-11	2.73
M-12	3.21	S-12	3.12

B. *In situ* experimental results

The values of the compensated acoustic time difference curve and the natural gamma logging curve measured according to the method in Sec. II D are shown in Fig. 7. The calculated effective porosities of the *in situ* formations are shown in Table III.

C. Thermal conductivities of *in situ* formation rock

The thermal conductivities of the *in situ* formation rocks as calculated using the ETG method are shown in Table IV.

IV. DISCUSSION

Based on the analysis of the effective porosity of the *in situ* strata in Table III, it can be seen that, except for a few geological formations, the effective porosities of other *in situ* strata were less than 5%. Considering Eq. (8), it was found that the main factors determining the thermal conductivity of the *in situ* rock were the thermal conductivity of the solid rock, the thermal conductivity of water, and the porosity of the formation. In a given formation, the porosity *in situ* and the thermal conductivity of the pore water are the only constants. Therefore, the main factor that determines the thermal conductivity of *in situ* rock is the thermal conductivity of the solid part of that rock.[12] In this study, the type and volume proportions of diagenetic minerals were analyzed by x-ray diffraction (XRD) experiments. Using the geometric-average model of the mineral composition, the solid-phase thermal conductivities of the rocks (λ_{s-XRD}) were predicted and fitted with Eq. (7) to establish the solid-phase thermal conductivity of the rock powder samples (λ_{s-TPS}) and to examine the accuracy of the TPS measurements of the solid-phase thermal conductivity of rock powder.

A. Geometric-mean model thermal conductivity predictions

Solid-phase rocks are composed of a variety of diagenetic minerals. According to the concept of circuit analysis, the thermal conductivity coefficients and volumes of each mineral can be regarded as multiple thermal conduction channels in parallel, as shown in Fig. 6(c). The geometric-average model of the mineral composition can then be used to predict the solid thermal conductivity using

$$\lambda_{s-XRD} = \prod_{i}^{n} \lambda_i^{x_i}, \tag{9}$$

where λ_{s-XRD} is the solid-phase thermal conductivity of rock obtained from its diagenetic mineral content, W/(m K); x_i is the volume percentage of mineral i in the sample—the value range of x_i is 0–1, and the values can be determined from Table III; n is the number of constituent rock mineral species—according to the results of XRD mineral analysis, the rock sample contained 11 kinds of diagenetic minerals, so n = 11; and λ_i is the thermal conductivity of mineral i, W/(m K), which can be found in Table VI. The lithogenic minerals in the table can be divided into five categories: silicoide, reticular silicate, zeolite, carbonate, and layered silicate.[23,24]

The cuttings were ground in the grinding instrument until the particle size was <0.075 mm, and mineral-component analysis tests were carried out by XRD [instrument model DX-2700, as shown in Fig. 3(d)]. According to the general rules of the JY/009-1996 rotating-target polycrystal XRD method, the measured XRD mineral spectral data were imported into the Jade 6.0 software package to determine the nature and volume fractions of diagenetic minerals, and the results are shown in Table V. Substituting the composition data from Table V and the thermodynamic data from Table VI into Eq. (7) gives the solid-phase thermal conductivities of the rock samples (λ_{s-XRD}), as shown in Fig. 8.

B. Solid-phase thermal conductivity fitting

Regarding geological age, from shallow to deep, the sampled strata belong to the Cretaceous Quantou Formation K_1q (depth range 700–1175 m), the Cretaceous Yingcheng Formation K_1y (depth range 1175–1525 m), and the Cretaceous Shihezi Formation K_1sh (depth range 1525–2000 m). The plots of λ_{s-TPS} and λ_{s-XRD} were fitted, and the fitting results are shown in Fig. 8. As shown in Fig. 8(a), the solid-phase thermal conductivities of rock obtained by the two methods were basically the same. Among these values, the solid-phase thermal conductivity of Shihezi Formation rock (K_1sh) had the highest coincidence degree, with differences in the range of 0.01–0.152 W/(m K). The second group was Quantou Formation rock, with a difference range of 0.026–0.165 W/(m K). The worst-fitting group was the Yingcheng Formation rocks, with a difference

TABLE V. Diagenetic mineral species and composition ratio.

	Volume fraction of mineral composition(%)										
$\lambda_{Mineral}$	7.69	2.31	2.14	0.391	3.59	5.57	2.02	1.9	1.9	5.14	2.6
No./Name	Quartz	Potassium feldspar	Anorthosite	Zeolite	Calcite	Dolomite	Biotite	Glimmerton	Illite/smectite formation	Chlorite	Kaolinite
M-1	11	7	8	⋯	10	8	⋯	2	54	⋯	⋯
M-2	16	2	12	⋯	5	6	⋯	1	56	⋯	2
M-3	17	2	35	⋯	5	5	⋯	1	35	⋯	⋯
M-4	27	2	25	⋯	⋯	5	2	2	37	⋯	⋯
M-5	24	2	14	⋯	2	5	⋯	10	30	13	⋯
M-6	16	1	10	⋯	5	1	⋯	5	60	2	⋯
M-7	22	7	20	⋯	8	⋯	⋯	5	29	9	⋯
M-8	21	5	15	⋯	⋯	⋯	⋯	10	38	11	⋯
M-9	21	⋯	13	⋯	2	3	⋯	12	37	12	⋯
M-10	24	2	15	⋯	⋯	⋯	⋯	12	34	13	⋯
M-11	16	⋯	13	4	10	7	2	16	10	20	2
M-12	8	⋯	20	⋯	15	⋯	2	10	10	35	4
S-1	23	15	12	⋯	2	⋯	2	2	44	⋯	⋯
S-2	38	14	30	⋯	⋯	⋯	2	⋯	16	⋯	⋯
S-3	38	⋯	12	5	2	13	1	20	6	2	1
S-4	27	10	15	⋯	3	2	⋯	7	28	8	⋯
S-5	24	1	17	7	6	4	⋯	10	21	10	⋯
S-6	25	⋯	16	⋯	10	1	⋯	10	26	12	⋯
S-7	24	⋯	25	⋯	5	5	3	21	9	8	⋯
S-8	24	14	16	⋯	2	1	⋯	12	16	15	⋯
S-9	21	10	15	⋯	10	⋯	2	10	14	18	⋯
S-10	18	12	20	⋯	11	1	3	8	7	20	⋯
S-11	31	⋯	10	⋯	5	⋯	1	10	35	8	⋯
S-12	25	⋯	37	⋯	5	3	4	12	⋯	14	⋯

TABLE VI. Thermodynamic parameters of diagenetic minerals.

	Mineral	λ [W/(m K)]
Silicoide	α-quartz	7.69
Reticular silicate	Potassium feldspar	2.31
	Anorthosite	2.14
Zeolite	Zeolite	0.39
Carbonate	Calcite	3.59
	Dolomite	5.57
Layered silicate	Biotite	2.02
	Glimmerton	1.90
	Illite/smectite formation	1.90
	Chlotite	5.14
	Kaolinite	2.60

range of 0.01–0.24 W/(m K). The differences in the thermal conductivities obtained by the two methods were normalized, and the results are shown in Fig. 8(b). The normalized values of more than 95% of these points were less than 0.1, and the normalized values of nearly 85% were less than 0.05.

By fitting the relationship between the thermal conductivity of the solid phase and the formation depth, it was found that the relationship between the two roughly conforms to a cubic curve. The following fitting curve was obtained:

$$y = 5.58x^3 - 2.12x^2 + 0.026x - 7.31, \tag{10}$$

where y is the solid-phase thermal conductivity, W/(m K), and x is the depth of the formation, m. This is plotted in Fig. 8(a).

To further examine these results, the SPSS 23.0 software package was used to conduct statistical analysis of the data obtained from the two methods. The measurement data were represented as $\bar{x} \pm s$, and the test data were in line with a normal distribution. An independent-samples t test was used for comparison between groups, and the resulting $P > 0.05$ indicates that there were no statistically significant differences. This indicates that the solid-phase

TABLE VII. Comparison of solid-phase thermal conductivities of rock samples determined by two methods ($\bar{x} \pm s$). Note: P = 0.56, obtained by independent-samples t test.

Measurement mode	Number of samples	Solid-phase thermal conductivity, W/(m K)
λ_{s-TPS}	24	3.11 ± 0.28
λ_{s-XRD}	24	3.16 ± 0.33

thermal conductivity values determined by the TPS method were basically consistent with those calculated by the geometric-average model. The statistical results are shown in Table VII.

In conclusion, the solid-phase thermal conductivities of rock obtained by TPS and a two-phase geometric-average model were accurate and reliable. This indirectly demonstrates that the method for determining the thermal conductivity of *in situ* formation rock using ETG is highly reliable.

V. CONCLUSIONS

(1) In this paper, a method for predicting the thermal conductivity of *in situ* rock using drilling cuttings is proposed. In this method, first, the thermal conductivity of solid-phase rock is predicted using a two-phase geometric-average model and the thermal conductivity of saturated cuttings measured using TPS. Then, the thermal conductivity of the solid-phase rock and the porosity of the *in situ* formation are substituted into the two-phase geometric-average model to predict the thermal conductivity of the *in situ* formation.

(2) This model can predict the thermal conductivity of *in situ* formation rock by measuring only the thermal conductivity of saturated cuttings, the porosity of saturated cuttings, and the porosity of the *in situ* formation. This is simple to operate and convenient for engineering applications.

(3) It was found by comparative statistical analysis of the results from the TPS and XRD methods, λ_{s-TPS} and λ_{s-XRD}, that the two methods correlate well. It was indirectly demonstrated

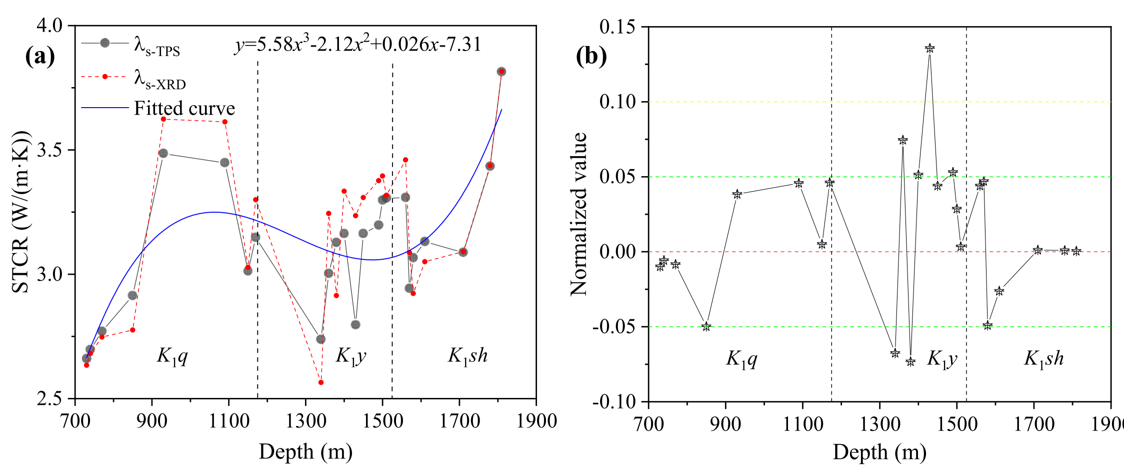

FIG. 8. Comparison of solid-phase rock thermal conductivity values: (a) fitting curve of solid-phase rock thermal conductivity; (b) normalization of fitting difference.

that the proposed method has high reliability, good feasibility, and high accuracy for predicting the thermal conductivity of *in situ* formation rock.

(4) The proposed method was used to predict the thermal conductivity of rocks *in situ* in the Cretaceous strata (within the range of 2000 m). The predicted thermal conductivity of sandstone was 2.40–3.69 W/(m K), and that of mudstone was 2.31–3.27 W/(m K).

ACKNOWLEDGMENTS

This project was supported by the National Natural Science Foundation of China (Grant No. 51774163) and the first batch of "Double First-class" discipline construction innovation teams of Liaoning Technical University (Grant No. LNTU20TD-26). The support is gratefully acknowledged.

DATA AVAILABILITY

The data that support the findings of this study are available from the corresponding author upon reasonable request.

REFERENCES

[1]Y. Zhang, S. Hao, Z. Yu *et al.*, "Comparison of test methods for shallow layered rock thermal conductivity between *in situ* distributed thermal response tests and laboratory test based on drilling in northeast China," Energy Build. **173**, 634–648 (2018).
[2]G. S. Jia, Z. Y. Tao, X. Z. Meng *et al.*, "Review of effective thermal conductivity models of rock-soil for geothermal energy applications," Geothermics **77**, 1–11 (2019).
[3]E. Zanchini, S. Lazzari, and A. Priarone, "Long-term performance of large borehole heat exchanger fields with unbalanced seasonal loads and groundwater flow," Energy **38**, 66–77 (2012).
[4]D. Barry-Macaulay, A. Bouazza, R. M. Singh *et al.*, "Thermal conductivity of soils and rocks from the Melbourne (Australia) region," Eng. Geol. **164**, 131–138 (2013).
[5]V. Pasquale, M. Verdoya, and P. Chiozzi, "Measurements of rock thermal conductivity with a transient divided bar," Geothermics **53**, 183–189 (2015).
[6]M. Kämmlein and H. Stollhofen, "Lithology-specific influence of particle size distribution and mineralogical composition on thermal conductivity measurements of rock fragments," Geothermics **80**, 119–128 (2019).
[7]X. Zhao, J. Cao, and H. Luo, "Experimental study on measuring thermal properties of rock and soil with hot disk," China Meas. Test **38**(4), 106–109 (2012).
[8]W. Pei, W. Yu, S. Li *et al.*, "A new method to model the thermal conductivity of soil–rock media in cold regions: An example from permafrost regions tunnel," Cold Reg. Sci. Technol. **95**, 11–18 (2013).
[9]G. Yang, Y. Yuan, Y. Shen *et al.*, "Analysis on thermal conductivity of cretaceous sandstone associated with microstructure," Coal Eng. **47**(9), 82–85 (2015).
[10]C. Iık, "Determination of the thermal conductivity of rock from P-wave velocity," Int. J. Rock Mech. Min. Sci. **41**, 703–708 (2004).
[11]P. Mielke, K. Bär, and I. Sass, "Determining the relationship of thermal conductivity and compressional wave velocity of common rock types as a basis for reservoir characterization," J. Appl. Geophys. **140**, 135–144 (2017).
[12]A. Tatar, S. Mohammadi, A. Soleymanzadeh, and S. Kord, "Predictive mixing law models of rock thermal conductivity: Applicability analysis," J. Pet. Sci. Eng. **197**, 107965 (2021).
[13]K. Golden and G. Papanicolaou, "Bounds for effective parameters of multicomponent media by analytic continuation," J. Stat. Phys. **40**(5/6), 655–666 (1985).
[14]F. L. Levy, "A modified Maxwell–Eucken equation for calculating the thermal conductivity of two-component solutions or mixtures," Int. J. Refrig. **4**(4), 223–225 (1981).
[15]L. Fiala, M. Jerman, P. Reiterman *et al.*, "Determination of thermal conductivity of silicate matrix for applications in effective media theory," Int. J. Thermophys. **39**(2), 28 (2018).
[16]O. Johansen, "Thermal conductivity of soils," Ph.D. thesis, Trondheim University, 1973.
[17]Z. Hashin and S. Shtrikman, "A variational approach to the theory of the effective magnetic permeability of multiphase materials," J. Appl. Phys. **33**(10), 3125–3131 (1962).
[18]J. Bi, M. Zhang, W. Chen *et al.*, "A new model to determine the thermal conductivity of fine-grained soils," Int. J. Heat Mass Transfer **123**, 407–417 (2018).
[19]M. Laurent, "Thermal properties of model foods in the frozen state," J. Food Eng. **15**(2), 83–97 (1992).
[20]Z. H. Zhang, J. T. Guo, X. F. Liu *et al.*, "SDZ-3000 computerized logging system," Pet. Instrum. **22**(2), 35–38 (2008).
[21]X. Luo, C. Q. Zhu, B. S. Zhang *et al.*, "Heat production rate calculation using gamma-ray logging of the sedimentary formation in the Tarim basin, Northwest China," Acta Geol. Sin. **94**(7), 2078–2088 (2020).
[22]F. Tong, L. Jing, and R. W. Zimmerman, "An effective thermal conductivity model of geological porous media for coupled thermo-hydro-mechanical systems with multiphase flow," Int. J. Rock Mech. Min. Sci. **46**(8), 1358–1369 (2009).
[23]F. Brigaud, G. Vasseur, and G. Caillet, "Thermal state in the north Viking Graben (North Sea) determined from oil exploration well data," Geophysics **57**(1), 69–88 (1992).
[24]C. Clauser and E. Huenges, "Thermal conductivity of rocks and minerals," in *Rock Physics and Phase Relations: A Handbook of Physical Constants* (AGU, Washington, D.C., 1995), Vol. 3, pp. 105–126.